JOINT EUROPEAN TORUS

JET–P(90)42

L-G. Eriksson, U. Willen, T. Hellsten and JET Team

Time Dependent Self-Consistent Calculations of ICRH-Power Deposition and Ion Velocity Distributions

Time Dependent Self-Consistent Calculations of ICRH-Power Deposition and Ion Velocity Distributions

L-G. Eriksson, U. Willen[1], T. Hellsten[2] and JET Team*

JET-Joint Undertaking, Culham Science Centre, OX14 3DB, Abingdon, UK

[1]Chalmers University of Technology, S-412%, Gothenburg, Sweden
[2]Royal Institute of Technology, 5-10044, Stockholm, Sweden
** See Appendix 1*

Preprint of a Paper Presented at the Joint Varenna-Lausanne International Workshop:
Theory of Fusion Plasmas, Varenna, Italy, 27-31 August 1990

TIME DEPENDENT SELF-CONSISTENT CALCULATIONS OF ICRH-POWER DEPOSITION AND ION VELOCITY DISTRIBUTIONS

L.-G. Eriksson, U. Willén[+] and T. Hellsten[*]

JET Joint Undertaking, Abingdon, Oxon. OX14 3EA, U.K.
[+]Chalmers University of Technology, S-41296, Gothenburg, Sweden
[*]Royal Institute of Technology, S-10044, Stockholm, Sweden

Abstract

A code for self-consistent time dependent calculations of the ICRH-power deposition and velocity distributions of the resonating ions in tokamaks has been developed. The basic principles behind the code and results from it are presented.

1. Introduction

Ion cyclotron resonance heating (ICRH) has become an often used heating method in tokamaks. In JET it is the main supplementary heating method with the potential of coupling about 25 MW of RF-power. The high power levels used in JET leads to a significant distortion of the velocity distributions of the resonating ions. The resulting distributions have non-Maxwellian anisotropic tails. These tails affect the dielectric properties of the plasma and hence the power deposition profile. The power deposition and the velocity distributions of the resonating ions must therefore be calculated self-consistently. Such self-consistent calculations has been done for steady state situations in Ref. [1]. However, the ion electron slowing down time, t_s, which is the characteristic time for ion tail development, can be up to 1-2 sec for typical JET scenarii. This means that t_s often is a large fraction of the RF-pulse duration and of the characteristic time for changes in the background plasma parameters. Thus, in order to

simulate a JET discharge one must in general do time dependent calculations. To solve this problem we have developed a code, called PION-T which calculates the ICRH-power deposition and ion velocity distributions self-consistently. The code is based on simplified models which makes the computing time reasonably short. It is therefore possible to use the code for routine analysis of discharges and in transport codes. A short description of the code and results from it are presented here.

2. Power Deposition Model

The flux surface integrated Poynting flux, $\overline{P}(s)$, for a single toroidal mode number is written as [2,3]

$$\overline{P}(s) = P_o\left[\kappa P_1(s) + (1-\kappa)P_2(s)\right] \tag{1}$$

$$\kappa = a_s^2(2-a_s) \tag{2}$$

$$P_1(s) = w_1 P_{1e}(s) + (1-w_1)P_{1i}(s) \tag{3}$$

$$P_2(s) = w_2 P_{2e}(s) + (1-w_2)P_{2i}(s) \tag{4}$$

Where a_s is the single pass absorption coefficient across the midplane and $s = \sqrt{\psi/\psi_a}$ (ψ is the poloidal flux and s = 1 at the boundary). In the above formulas P_{1e} and P_{2e} represent the flux absorbed directly by the electrons via TTMP/ELD, whereas P_{1i} and P_{2i} represent the flux absorbed by the ions via ion cyclotron absorption. For details about P_{1e}, P_{2e}, w_1 and w_2 see Ref. [3]. The P_{1i} function representing single pass damping is given by

$$p_{1i}(s) = \sum_{\alpha}(a_\alpha/a_s)p_{1\alpha}(s) \tag{5}$$

$$p_{1\alpha}(s) = \left\{1-\exp\left[-(s/s_{o\alpha})^2 \ell n2\right]\right\} \Big/ \left\{1-\exp\left[-(1/s_{o\alpha})^2 \ell n2\right]\right\} \tag{6}$$

where α should sum over the resonant ion species and a_α is the contribution from ion species α to a_s. The width $s_{o\alpha}$ is mainly determined by the parameter $d_\alpha^2 = (n_\phi/\omega r_o)^2 \langle v_\parallel^2 \rangle_\alpha$ [2] where n_ϕ is the toroidal mode number, $\langle v_\parallel^2 \rangle_\alpha$ is the averaged squared parallel velocity of species α and r_o the minor radius at the outboard side. The P_{2i} function represents weak ion damping and is obtained from

$$P_{2i}(s)=\sum_{\alpha}P_{2\alpha}(s)=\sum_{\alpha}\int_0^s a_\alpha(\xi)f(\xi)d\xi\Big/\sum_{\alpha}\int_0^1 a_\alpha(\xi)f(\xi)d\xi \tag{7}$$

where $a_\alpha(s)$ is the single pass absorption coefficient for ion species α across the resonance at the flux surface s and f(s) is a calibration function [2]. In order to save computing time we use the WKB approximation when calculating $a_\alpha(s)$ but a more accurate calculation can in principle be used. Using the WKB approximation one has

$$a_\alpha(s)=\omega\int_{-\infty}^{\infty}\mathrm{Im}\left(\vec{E}^{*}\vec{\vec{\varepsilon}}_\alpha\vec{E}\right)dx/(2\pi P_x)=\int_{-\infty}^{\infty}\frac{k_o^2}{|k_\perp|}\left\{\mathrm{Im}\left(\varepsilon_{xx}^{\alpha}\right)\left|\frac{\varepsilon_{xy}}{\varepsilon_{xx}-n_\parallel^2}\right|^2+\mathrm{Im}\left(\varepsilon_{xy}^{\alpha}\right)\right.$$
$$\left.+2\,\mathrm{Re}\left(\varepsilon_{xy}^{\alpha}\right)\mathrm{Im}\left[\frac{\varepsilon_{xy}}{\varepsilon_{xx}-n_\parallel^2}\right]\right\}\exp\left[\int_{-\infty}^{\infty}2\,\mathrm{Im}\left(k_\perp(x')\right)dx'\right]dx \tag{8}$$

where x is the direction across the resonance and perpendicular to the magnetic field.

The total power deposition is obtained by summing the power depositions for the individual n_ϕ weighted with an antenna spectrum.

3. Fokker-Planck Equation

The Fokker-Planck equation can be written as [4]

$$\frac{\partial f}{\partial t}=C(f)+Q(f) \tag{9}$$

where C(f) is the collision operator and Q(f) is the RF-operator.

In order to simplify the problem we only calculate the pitch angle averaged velocity distribution function F(v). We use the following approximate equation to calculate F(v) [5]

$$\frac{\partial F}{\partial t}=\frac{1}{\mathrm{v}^2}\frac{\partial}{\partial \mathrm{v}}\left[-\alpha\mathrm{v}^2+\frac{1}{2}\frac{\partial}{\partial \mathrm{v}}\left(\beta\mathrm{v}^2\right)\right]+\frac{1}{\mathrm{v}^2}\frac{\partial}{\partial \mathrm{v}}\left[\mathrm{v}^2H\left(\frac{k_\perp \mathrm{v}}{\omega_{\mathrm{ci}}}\right)\frac{\partial F}{\partial \mathrm{v}}\right] \tag{10}$$

$$H=\frac{1}{2}\int_{-1}^{1}K\left|J_{n-1}\left(\frac{k_\perp \mathrm{v}}{\omega_{\mathrm{ci}}}\sqrt{1-\mu^2}\right)+(E_-/E_+)J_{n+1}\left(\frac{k_\perp \mathrm{v}}{\omega_{\mathrm{ci}}}\sqrt{1-\mu^2}\right)\right|^2 d\mu \tag{11}$$

where α and β are given in Ref. [4], K is a constant proportional to $|E_+|^2$ and E_+ and E_- are the left and right hand polarized components of the electric field respectively. The quantity $<v_\parallel^2>_\alpha$ needed in the power deposition calculation is obtained from the following formula [6]:

$$< v_\parallel^2 >= \int_0^\infty \mu_{eff}^2 v^2 F(v) 4\pi v^2 dv \tag{12}$$

$$\mu_{eff}^2 = (1/3)\left[1+(v/v_*)^2\right]\Big/\left[1+(v/v_*)^2+1+(v/v_*)^4\right] \tag{13}$$

with $v_* \equiv 0.5\, v_\gamma$ where v_γ is the characteristic velocity where the pitch angle scattering becomes weak [4].

4. Self-Consistent Calculations

The velocity distribution of the resonating ions affects the power deposition in mainly two ways: (i) the parallel velocity component determines the Doppler broadening of the cyclotron resonance and to some extent the absorption strength; (ii) the perpendicular velocity component mainly affects the absorption strength. Thus, we need to calculate $<v_\parallel^2>_\alpha$ and the absorption strength self-consistently. The latter means that the following two expressions for the locally absorbed power must give the same result.

$$p_{f\alpha}(\vec{E}) = \frac{\omega}{2\pi}\mathrm{Im}\left(\vec{E}^*\vec{\vec{\varepsilon}}_\alpha\vec{E}\right) \tag{14}$$

and

$$p_{f\alpha}(\vec{E}) = \int 0.5\, m v^2 Q(f_\alpha) d^3v \tag{15}$$

For a given distribution function we calculate $<v_\parallel^2>_\alpha$ from Eq. (12), and the absorption strength in the power deposition calculation is made to agree with that of the Fokker-Planck calculation with the following procedure: calculate the dielectric tensor, $\vec{\vec{\varepsilon}}_{o\alpha}$, including absorption to lowest order in $k_\perp v_\perp/\omega_{ci}$ and the locally absorbed power $p_{o\alpha}$ for a bi-Maxwellian velocity distribution with the same density and parallel temperature as the actual distribution but with the perpendicular temperature equal to the background ion temperature. Then calculate

$$\gamma_\alpha = p_{f\alpha}/p_o \tag{16}$$

$$\gamma_t = \sum_\alpha \gamma_\alpha \left[da_{\alpha o}/dx \right] \Big/ \sum_\alpha \left[da_{\alpha o}/dx \right] \qquad (17)$$

where $p_{f\alpha}$ is the power absorbed by the actual distribution function from Eq. (15) and $a_{\alpha o}$ is the absorption coefficient obtained from Eq. (8) with $\vec{\vec{\varepsilon}}_o$ as the dielectric tensor. The actual absorption coefficient is then obtained by multiplying the integrand of Eq. (8) with γ_α and replacing $\mathrm{Im}(k_\perp)$ with $\gamma_t\ \mathrm{Im}(k_\perp)$, but still using $\vec{\vec{\varepsilon}}_o$ as the dielectric tensor.

With the above outlined procedure we avoid calculating the actual dielectric tensor, which is much more complicated.

The PION-T code works as follows: at the beginning of each time step the parameters $\langle v_\parallel^2 \rangle_\alpha$, γ_α and γ_t are evaluated from the distribution function, a power deposition is produced and the ratio E_-/E_+ is calculated; the evolution of the distribution function is then calculated during the time step keeping the power deposition fixed; from the distribution function at the end of the time step, i.e. at the beginning of a new time step, a new set of parameters $\langle v_\parallel^2 \rangle_\alpha$, γ_α and γ_t is evaluated and a new power deposition is calculated; this procedure is repeated until the end of the calculation.

5. Examples

First we study the response to a step in RF-power for the following two test cases:

(i) Second harmonic heating of tritium in a DT plasma, $n_T = n_D = 2.5 \cdot 10^{19}(1\text{-}0.9S^2)^{0.55} m^{-3}$, $T_e = T_i = 8\ (1\text{-}0.9S^2)^2 keV$, $B_o = 3.24$ T, $f = 33$ MHz, Dipole antenna (i.e. the antenna spectrum peaks at higher toroidal mode numbers in this case around $n_\phi = 30$).

(ii) Fundamental minority heating of deuterium in a tritium plasma, $n_D = 0.15\ n_T$, $n_T = 4.35 \cdot 10^{19}(1\text{-}0.9S^2)^{0.55} m^{-3}$, $T_e = T_i = 8\ (1\text{-}0.9S^2)^2 keV$, $B_o = 3.27$ T, $f = 25$ MHz, Dipole antenna.

An RF-power of 10 MW is switched on at t = 0.1 s and then switched off at t = 2.0 s. The background parameters are kept constant. A plasma size typical for JET is used. Figs. 1-6 shows the response of a number of quantities. In Fig. 1 the RF-power absorbed via ion cyclotron damping by the ions and via TTMP/ELD by the electrons is shown for case (i). At the beginning

of the RF-pulse the ion cyclotron absorption is weak and most of the power goes directly to the electrons. However, as the tritium distribution develops a tail, the ion cyclotron damping becomes stronger and dominates at the end. The enhanced absorption is due to the fact that second harmonic absorption is a finite Larmor radius effect and therefore very sensitive to the shape of the distribution function. It can also be seen in Fig. 1 that the RF-powers absorbed by the ions and the electrons reaches steady levels after about a slowing down time. A similar type of behaviour can be seen in Fig. 2 for case (ii) but the change in ion cyclotron absorption is not as dramatic as for case (i).

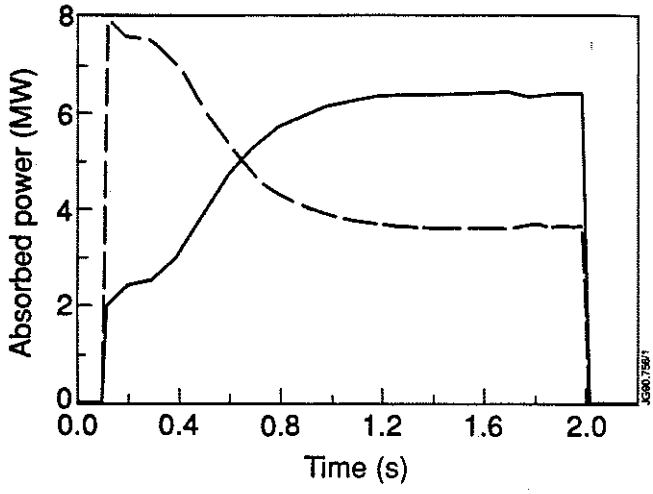

Fig. 1: RF-power absorbed by the tritium ions (—) and by the electrons (----) for case (i).

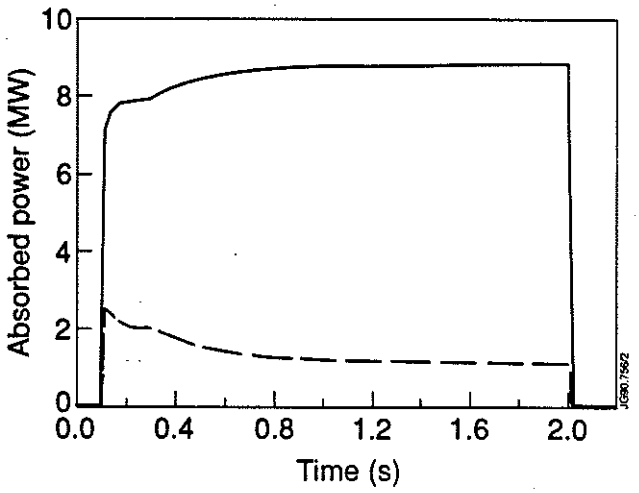

Fig. 2: RF-power absorbed by the deuterium ions (—) and by electrons (----) for case (ii).

The difference is that the ion cyclotron damping for case (ii) is strong even for a Maxwellian distribution. For case (ii) the enhanced ion absorption is due to the E_- component of the electric field which mainly affects the tail ions. Fig. 3 shows the flux surface integrated Poynting flux for case (i) as a function of s for a number of time points. As can be seen the power deposition becomes more peaked as the ion cyclotron absorption increases due to the developing tritium tail. In Fig. 4 the collisional power transfer from the resonating ions to the background ions and electrons for case (ii) is shown.

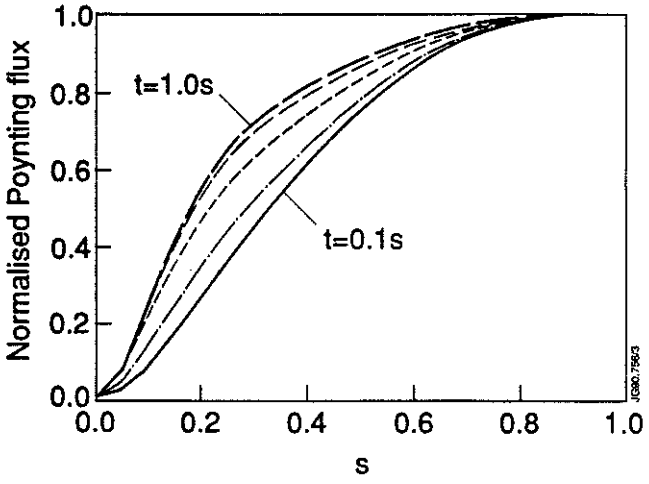

Fig. 3: Flux surface integrated Poynting flux for case (i) at t = 0.1, 0.4, 0.6, 0.8, and 1.0s.

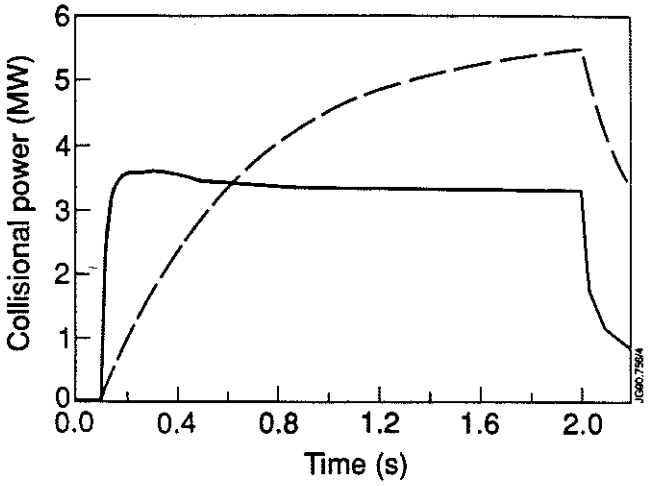

Fig. 4: Power transferred from the resonating ions to the ions (—) and to the electrons (---) for case (ii).

As can be seen, the time scale for the transfer to the ions is much shorter than to the electrons. Figs. 5 and 6 show the fusion reactivity for the two cases. In case (i) the fusion reactivity reaches a peak even before the absorbed power has reached a steady level.

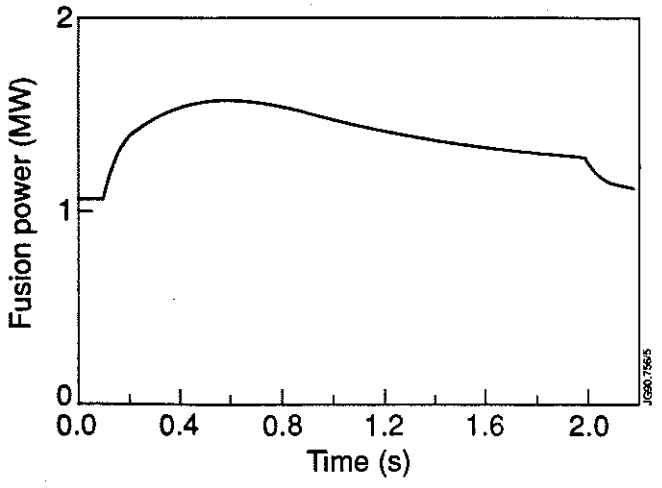

Fig. 5: Fusion power for case (i).

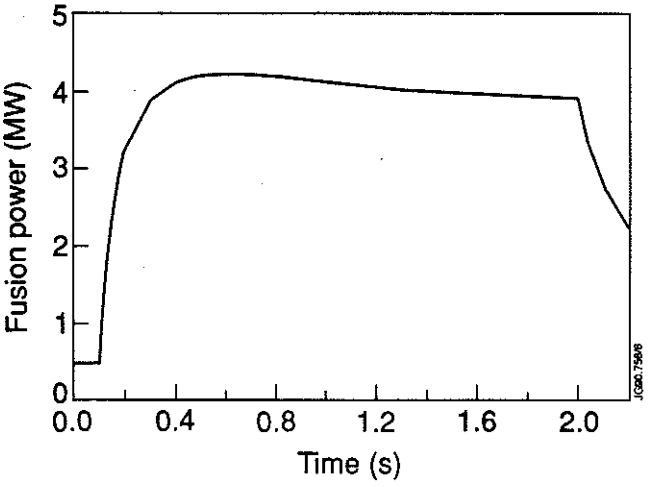

Fig. 6: Fusion power for case (ii).

This effect is caused by ions being pushed above the peak of the fusion cross section (which is around 100 keV for cases (i) and (ii)). A higher gain in fusion reactivity from the developing tail is obtained for case (ii) than for case (i). The reason for this is that second harmonic heating mainly accelerates particles with high velocities and therefore creates tails with more particles above the maximum of the cross-section.

The code has also been used to study the collisional power transfer to the electrons during RF-power modulation. A case with minority heating of ^3He in a deuterium plasma has been studied. The parameters, which are typical for a modulation experiment at JET are as follows: $n_{3He} = 7.10^{17}(1-0.9S^2)^{0.55}m^{-3}$,$nD = 2.6.10^{19}(1-0.9S^2)^{0.55}m^{-3}$,$T_i = T_e = 8(1-0.9S^2)^6$keV,B = 3.24T,f = 33MHz. Fig. 7 shows the power absorbed and collisionally transferred to the electrons. In Fig. 8 the profiles of the stationary and modulated power transfer are shown. The modulated power transfer profile is much broader than the stationary, which is an effect of the peaked temperature profile.

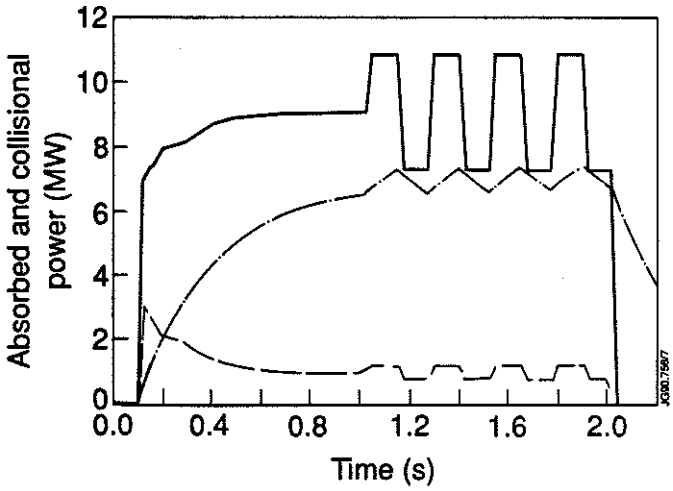

Fig. 7: RF-power absorbed by the helium ions (—) and by the eletrons (---), transferred power to the eletrons (– - –).

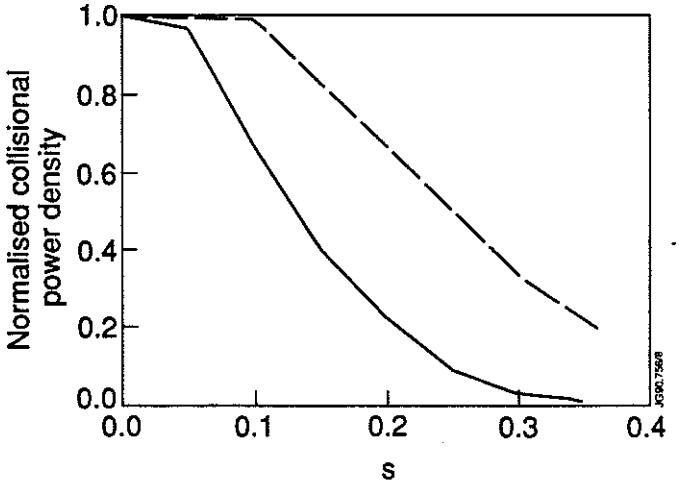

Fig. 8: Power density transferred from the resonating ions to the electrons versus s stationary (—) modulated (---).

6. Conclusions

We have developed a code for time dependent self-consistent calculations of ICRH-power deposition and ion velocity distributions. Since the code is based on simplified models the computing time becomes reasonably short. However, the use of simplified models also means that the code has limitation. The most essential limitations are: the neglect of effects caused by the finite widths of the banana orbits of the trapped high energy ions; the neglect of RF-induced spatial diffusion. Cases where very energetic ions are present can therefore not be treated properly.

It has been demonstrated that the effect of the velocity distribution plays an important role on the power deposition. Specifically the scenario with second harmonic heating of tritium is strongly affected by the developing tail of the distribution function. The power deposition profiles have been shown to reach steady state on the time scale of a slowing down time. In a comparison between second harmonic heating of tritium in a DT plasma and fundamental minority heating of deuterium in a tritium plasma the latter scenario has been found to be more efficient for producing fusion reactions. It is interesting to note that the fusion reaction rate peaks before the ion tails are fully developed for the two scenarii. This effect is due to the resonating ions being pushed beyond the maximum of the fusion cross-section. During ICRH-power modulation the profile of the collisional power transfer from the resonating ions to the electrons can be much broader for the modulated part than for the stationary.

References

[1] L.-G. Eriksson, T. Hellsten et al., Nuclear Fusion 29 (1989) 87.

[2] T. Hellsten and L. villard, Nuclear Fusion 28 (1988) 285.

[3] T. Hellsten and L.-G. Eriksson, Nuclear Fusion 29 (1989) 2165.

[4] T.H. Stix, Nuclear Fusion 15 (1975) 737.

[5] D. Anderson, W.G.F. Core, L.-G. Eriksson, H. Hamnén, T. Hellsten and M. Lisak, Nuclear Fusion 27 (1987) 911.

[6] D. Anderson, L.-G. Eriksson and M. Lisak, Plasma Physics and Controlled Fusion 29 (1987) 891.

APPENDIX 1.

THE JET TEAM

JET Joint Undertaking, Abingdon, Oxon, OX14 3EA, U.K.

J.M.Adams[1], F.Alladio[4], H.Altmann, R.J.Anderson, G.Appruzzese, W.Bailey, B.Balet, D.V.Bartlett, L.R.Baylor[24], K.Behringer, A.C.Bell, P.Bertoldi, E.Bertolini, V.Bhatnagar, R.J.Bickerton, A.Boileau[3], T.Bonicelli, S.J.Booth, G.Bosia, M.Botman, D.Boyd[31], H.Brelen, H.Brinkschulte, M.Brusati, T.Budd, M.Bures, T.Businaro[4], H.Buttgereit, D.Cacaut, C.Caldwell-Nichols, D.J.Campbell, P.Card, J.Carwardine, G.Celentano, P.Chabert[27], C.D.Challis, A.Cheetham, J.Christiansen, C.Christodoulopoulos, P.Chuilon, R.Claesen, S.Clement[30], J.P.Coad, P.Colestock[6], S.Conroy[13], M.Cooke, S.Cooper, J.G.Cordey, W.Core, S.Corti, A.E.Costley, G.Cottrell, M.Cox[7], P.Cripwell[13], F.Crisanti[4], D.Cross, H.de Blank[16], J.de Haas[16], L.de Kock, E.Deksnis, G.B.Denne, G.Deschamps, G.Devillars, K.J.Dietz, J.Dobbing, S.E.Dorling, P.G.Doyle, D.F.Düchs, H.Duquenoy, A.Edwards, J.Ehrenberg[14], T.Elevant[12], W.Engelhardt, S.K.Erents[7], L.G.Eriksonn[5], M.Evrard[2], H.Falter, D.Flory, M.Forrest[7], C.Froger, K.Fullard, M.Gadeberg[11], A.Galetsas, R.Galvao[8], A.Gibson, R.D.Gill, A.Gondhalekar, C.Gordon, G.Gorini, C.Gormezano, N.A.Gottardi, C.Gowers, B.J.Green, F.S.Griph, M.Gryzinski[26], R.Haange, G.Hammett[6], W.Han[9], C.J.Hancock, P.J.Harbour, N.C.Hawkes[7], P.Haynes[7], T.Hellsten, J.L.Hemmerich, R.Hemsworth, R.F.Herzog, K.Hirsch[14], J.Hoekzema, W.A.Houlberg[24], J.How, M.Huart, A.Hubbard, T.P.Hughes[32], M.Hugon, M.Huguet, J.Jacquinot, O.N.Jarvis, T.C.Jernigan[24], E.Joffrin, E.M.Jones, L.P.D.F.Jones, T.T.C.Jones, J.Källne, A.Kaye, B.E.Keen, M.Keilhacker, G.J.Kelly, A.Khare[15], S.Knowlton, A.Konstantellos, M.Kovanen[21], P.Kupschus, P.Lallia, J.R.Last, L.Lauro-Taroni, M.Laux[33], K.Lawson[7], E.Lazzaro, M.Lennholm, X.Litaudon, P.Lomas, M.Lorentz-Gottardi[2], C.Lowry, G.Magyar, D.Maisonnier, M.Malacarne, V.Marchese, P.Massmann, L.McCarthy[28], G.McCracken[7], P.Mendonca, P.Meriguet, P.Micozzi[4], S.F.Mills, P.Millward, S.L.Milora[24], A.Moissonnier, P.L.Mondino, D.Moreau[17], P.Morgan, H.Morsi[14], G.Murphy, M.F.Nave, M.Newman, L.Nickesson, P.Nielsen, P.Noll, W.Obert, D.O'Brien, J.O'Rourke, M.G.Pacco-Düchs, M.Pain, S.Papastergiou, D.Pasini[20], M.Paume[27], N.Peacock[7], D.Pearson[13], F.Pegoraro, M.Pick, S.Pitcher[7], J.Plancoulaine, J-P.Poffé, F.Porcelli, R.Prentice, T.Raimondi, J.Ramette[17], J.M.Rax[27], C.Raymond, P-H.Rebut, J.Removille, F.Rimini, D.Robinson[7], A.Rolfe, R.T.Ross, L.Rossi, G.Rupprecht[14], R.Rushton, P.Rutter, H.C.Sack, G.Sadler, N.Salmon[13], H.Salzmann[14], A.Santagiustina, D.Schissel[25], P.H.Schild, M.Schmid, G.Schmidt[6], R.L.Shaw, A.Sibley, R.Simonini, J.Sips[16], P.Smeulders, J.Snipes, S.Sommers, L.Sonnerup, K.Sonnenberg, M.Stamp, P.Stangeby[19], D.Start, C.A.Steed, D.Stork, P.E.Stott, T.E.Stringer, D.Stubberfield, T.Sugie[18], D.Summers, H.Summers[20], J.Taboda-Duarte[22], J.Tagle[30], H.Tamnen, A.Tanga, A.Taroni, C.Tebaldi[23], A.Tesini, P.R.Thomas, E.Thompson, K.Thomsen[11], P.Trevalion, M.Tschudin, B.Tubbing, K.Uchino[29], E.Usselmann, H.van der Beken, M.von Hellermann, T.Wade, C.Walker, B.A.Wallander, M.Walravens, K.Walter, D.Ward, M.L.Watkins, J.Wesson, D.H.Wheeler, J.Wilks, U.Willen[12], D.Wilson, T.Winkel, C.Woodward, M.Wykes, I.D.Young, L.Zannelli, M.Zarnstorff[6], D.Zasche[14], J.W.Zwart.

PERMANENT ADDRESS

1. UKAEA, Harwell, Oxon. UK.
2. EUR-EB Association, LPP-ERM/KMS, B-1040 Brussels, Belgium.
3. Institute National des Récherches Scientifique, Quebec, Canada.
4. ENEA-CENTRO Di Frascati, I-00044 Frascati, Roma, Italy.
5. Chalmers University of Technology, Göteborg, Sweden.
6. Princeton Plasma Physics Laboratory, New Jersey, USA.
7. UKAEA Culham Laboratory, Abingdon, Oxon. UK.
8. Plasma Physics Laboratory, Space Research Institute, Sao José dos Campos, Brazil.
9. Institute of Mathematics, University of Oxford, UK.
10. CRPP/EPFL, 21 Avenue des Bains, CH-1007 Lausanne, Switzerland.
11. Risø National Laboratory, DK-4000 Roskilde, Denmark.
12. Swedish Energy Research Commission, S-10072 Stockholm, Sweden.
13. Imperial College of Science and Technology, University of London, UK.
14. Max Planck Institut für Plasmaphysik, D-8046 Garching bei München, FRG.
15. Institute for Plasma Research, Gandhinagar Bhat Gujat, India.
16. FOM Instituut voor Plasmafysica, 3430 Be Nieuwegein, The Netherlands.
17. Commissiariat à L'Energie Atomique, F-92260 Fontenay-aux-Roses, France.
18. JAERI, Tokai Research Establishment, Tokai-Mura, Naka-Gun, Japan.
19. Institute for Aerospace Studies, University of Toronto, Downsview, Ontario, Canada.
20. University of Strathclyde, Glasgow, G4 ONG, U.K.
21. Nuclear Engineering Laboratory, Lapeenranta University, Finland.
22. JNICT, Lisboa, Portugal.
23. Department of Mathematics, Univeristy of Bologna, Italy.
24. Oak Ridge National Laboratory, Oak Ridge, Tenn., USA.
25. G.A. Technologies, San Diego, California, USA.
26. Institute for Nuclear Studies, Swierk, Poland.
27. Commissiariat à l'Energie Atomique, Cadarache, France.
28. School of Physical Sciences, Flinders University of South Australia, South Australia SO42.
29. Kyushi University, Kasagu Fukuoka, Japan.
30. Centro de Investigaciones Energeticas Medioambientales y Techalogicas, Spain.
31. University of Maryland, College Park, Maryland, USA.
32. University of Essex, Colchester, UK.
33. Akademie de Wissenschaften, Berlin, DDR.

CR 88.49.1A